Remote Sens. **2015**, *7*, 15702-15728; doi:10.3390/rs71115702

OPEN ACCESS

remote sensing

ISSN 2072-4292

www.mdpi.com/journal/remotesensing

Article

On the Use of Global Flood Forecasts and Satellite-Derived Inundation Maps for Flood Monitoring in Data-Sparse Regions

Beatriz Revilla-Romero [1,2,*], Feyera A. Hirpa [1], Jutta Thielen-del Pozo [1], Peter Salamon [1], Robert Brakenridge [3], Florian Pappenberger [4,5] and Tom De Groeve [1]

1 European Commission, Joint Research Centre, Ispra 21027, Italy;
E-Mails: feyera-aga.hirpa@jrc.ec.europa.eu (F.A.H.); jutta.thielen@jrc.ec.europa.eu (J.T.); peter.salamon@jrc.ec.europa.eu (P.S.); tom.de-groeve@jrc.ec.europa.eu (T.D.G.)

2 Faculty of Geosciences, Utrecht University, Utrecht 3508, The Netherlands

3 Institute of Arctic and Alpine Research (INSTAAR), University of Colorado, Boulder, CO 80309, USA; E-Mail: robert.brakenridge@colorado.edu

4 European Centre For medium-range Weather Forecast, Reading RG2 9AX, UK;
E-Mail: florian.pappenberger@ecmwf.int

5 School of Geographical Sciences, University of Bristol, Bristol, BS8 1SS, UK

***** Author to whom correspondence should be addressed; E-Mail: b.revillaromero@gmail.com; Tel.: +44-755-27-47-316.

Academic Editors: Guy J-P. Schumann, Magaly Koch and Prasad S. Thenkabail

Received: 25 August 2015 / Accepted: 17 November 2015 / Published: 23 November 2015

Abstract: Early flood warning and real-time monitoring systems play a key role in flood risk reduction and disaster response decisions. Global-scale flood forecasting and satellite-based flood detection systems are currently operating, however their reliability for decision-making applications needs to be assessed. In this study, we performed comparative evaluations of several operational global flood forecasting and flood detection systems, using 10 major flood events recorded over 2012–2014. Specifically, we evaluated the spatial extent and temporal characteristics of flood detections from the Global Flood Detection System (GFDS) and the Global Flood Awareness System (GloFAS). Furthermore, we compared the GFDS flood maps with those from NASA's two Moderate Resolution Imaging Spectroradiometer (MODIS) sensors. Results reveal that: (1) general agreement was found between the GFDS and MODIS flood detection systems, (2) large differences exist in the spatio-temporal characteristics of the GFDS detections and GloFAS forecasts, and (3) the quantitative validation of global flood disasters in data-sparse regions is highly challenging.

Overall, satellite remote sensing provides useful near real-time flood information that can be useful for risk management. We highlight the known limitations of global flood detection and forecasting systems, and propose ways forward to improve the reliability of large-scale flood monitoring tools.

Keywords: Global hydrology; flood detection; flood monitoring; flood forecasting; disaster response; natural hazards; GFDS; MODIS; GloFAS

1. Introduction

Floods are among the most catastrophic natural disasters globally in terms of impact on human life and the economy. For example, in the last two decades, they accounted for 55% of people affected [1] and caused a major share of the economic damages. Even though flooding is a global phenomenon, Asia and Africa were worse hit by flood damages compared to other continents due not only to the higher frequency or magnitude of the flood events, but also due to the more exposed and vulnerable societies, and the lack of coping capacity of the institutions in these continents [2]. In light of mitigating the impacts, global scale flood risk reduction measures such as early warning systems (e.g., flood forecasting systems), and satellite-based real-time detection and monitoring tools have been developed in the last decade. In partnership [3] with international flood disaster response organizations and end-users, these measures [4–7] are useful to increase awareness of upcoming and ongoing flooding and contribute to improved flood disaster management.

To be used at their full potential, it is essential that end users can assess the reliability of these data services and processing systems in terms of whether they correctly represent the flood occurrence and characteristics on the ground. For example, humanitarian sectors need to know the skill of the forecasting or detection systems if they are to be used in decision-making for action [8,9]. However, any global-scale validation of these systems is hampered by the lack or limited availability of *in situ* streamflow in many areas of the world [10,11]. This constraint is even more acute for validation of real-time flood forecasts. For instance, from the 2692 global stations with some daily streamflow data available between 2011 and 2015 currently provided by the Global Runoff Data Centre[11], only ~0.2% of these stations are located outside Europe, North America, Australia and South Africa. This indicates that either the vast majority of the globe is without recent updates of streamflow data or that the data collected at the national level is not being shared publicly.

To fill this gap, data from satellite remote sensing of surface water extent and levels have been considered either as a complementary, or an alternative to *in situ* measurements[12,13]. In several applications, they have successfully been used as a proxy of streamflow [14–18], for model calibration and/or validation [19–24], and hydrologic data assimilation [20–23]. For example, data from satellite passive microwave sensors have been used for detecting flooded areas [24–29], and satellite altimeters have been used to estimate water surface elevation [30–32]. Other applications based on satellite-derived data, and beneficial for flood models, are related to better values for topographic elements such as river channel width [33] and depth [34,35].

Flooding can occur due to various phenomena. Coastal flood is caused by storm surges, sea level rise or tsunami wave; riverine flood normally occurs as a result of heavy rainfall in the upstream areas of a catchment causing an inundation of a normally dry area due to high water volumes (levels) in river streams; flash flood is caused by heavy rainfall in short period of time or a sudden release of dams; and more flood inundation could occur due to lake overflow or groundwater level rise. Different modelling and measurement approaches are needed to forecast or detect each of the various flood types. For instance, hydrological models used for flood forecasting typically focus on riverine floods (streamflow volume and hazard maps) while most satellite sensors detect flood inundated areas which could be results of riverine floods, flash floods, lake expansion or other changes in water surface area.

At global scale, the most commonly used flood inundation maps are derived from passive microwave sensors [14,36] or from Moderate Resolution Imaging Spectroradiometer (MODIS) imagery [16]. The Global Flood Detection System (GFDS) is an experimental system set up to detect and map in near-real time major river floods based on daily passive microwave satellite observations, on daily basis at a spatial resolution of $0.09° \times 0.09°$. The GFDS is being used to monitor ongoing floods by several international organizations. It has been previously used for a multi-satellite validation study [37] for the flood event in Pakistan in 2010 and compared to social media information for Pakistan and Philippines flood disasters in 2014 [38]. It was found that the GFDS flood signal is well correlated with the *in situ* streamflow for the 2010 Indus river flood in Pakistan [37]. Another near real-time global flood mapping is based on optical imagery from MODIS [39] produced at 250 m spatial resolution and at daily time steps. Although the GFDS and MODIS datasets are valuable sources of land surface hydrological information, especially due to their global coverage, open data policy and the advantage of being available at frequent temporal intervals and shortly after the satellite image retrieval, there is a need for evaluating their reliability for disaster management/response purposes.

Previous evaluation studies are focused on smaller scales (e.g., basin scale), and have shown a fairly good agreement between remotely sensed flood extent and *in situ* streamflow, in cases where the latter is available [16,40]. Moreover, it has been noted [37] that data from multispectral and microwave remote sensors is useful for supplementation of stream gauges in sparsely gauged basins. Other studies have used inundation extents derived from relatively higher resolution (30m) Landsat TM/ETM+ images as the "ground truth" to evaluate MODIS images [41–43], and they found an agreement of 73%–97% between the two products for those case studies. However, it should be noted that the Landsat revisit time is 16 days, and therefore has a potential of missing shorter flood events. Furthermore, streamflow time series from model simulations have been used for improving the flood inundation maps from satellite-remote sensing [42,44,45]. Finally, it is evident that it is a challenging task to do a global scale validation of flood inundation extent because of the lack of reliable validation data during the time period of flood event [46].

In this study, we use probabilistic streamflow forecasts from the Global Flood Awareness System (GloFAS) [4] for comparatively evaluating the remotely sensed flood maps using 10 riverine flood cases obtained from global flood databases [47,48]. The flood databases mainly contain information related to flood hazard (intensity, extent and duration), and standards for recording and sharing disaster loss and damage data [49] are under development. All the case studies are located in Africa, Asia, or South America, all of which are traditionally regions with limited up-to-date *in situ* streamflow

data [50]. Our study focuses on major events since these are likely to be reported in media, and archived in the disaster databases.

The overarching objective of this study is to investigate the skills of the detection and forecasting systems in correctly characterizing the flood events (in terms of their extent, location, and duration). Specifically, we aim to evaluate the usability of the global scale detection and forecasting systems for operational flood monitoring, and outline the limitations of each system. In Section 2 we present the study regions, the flood case studies and the data used. Section 3 explains the methodologies related to the satellite data and the hydrologic model, as well as the assessment procedures. Results and discussion are presented in Sections 4 and 5, respectively, and conclusions are summarized in Section 6.

2. Study Regions and Data

The evaluation study was carried out using major flood events selected from global flood archives. The details of the study regions and data used are described as follows.

2.1. Flood Disaster Databases and Case Studies

We selected ten major flood events that occurred in data-sparse regions during a three-year period, between 2012 and 2014 (Figure 1, Table 1). The selected riverine floods were caused by heavy or monsoonal rainfall and have a reported duration of at least 15 days. All events were recorded in the Dartmouth Flood Observatory (DFO) Archive [47] and the Emergency Database (EM-DAT) [48]. While DFO archive exclusively focuses on flood hazards and it is more comprehensive, the EM-DAT database records all kinds of disasters that fulfill at least one of their criteria: ten or more people killed; hundreds or more reported affects; declaration of a state of emergency; or a call for international assistance.

The DFO archive maintains a historical list of major global flood events since 1985 based on various news, governmental, instrumental, and remote sensing sources. The archive includes information such as the start and end dates of a flood event, estimates of affected area, approximate centroid of the affected area, and the severity and damages caused by the flood disasters. The global map of flood affected areas (which may not be actual flooded areas) are produced by the DFO based upon information acquired from news sources [47].

The EM-DAT flood database also provides a list of historical global flood disasters covering a longer time period (more than 100 years) that includes the duration of the flood, impacted area, and damages caused. For this study, the maps of impacted area for the selected flood disasters were provided by the Centre for Research on the Epidemiology of Disasters (CRED), which maintains the EM-DAT. The impacts of the flood disasters in the EM-DAT database is georeferenced based on the administrative units of the population and/or infrastructure impacted, which may not directly correspond to the footprint of the flood hazard. We use these impacted area maps produced for the 10 case studies, but it should be noted that the administrative units usually cover larger geographical area than the flood inundations, and should be carefully used.

Note that throughout this paper, we define the affected area as the area affected by the flood hazard, in agreement with DFO definition when satellite mapping is used, and the impacted area as the area where the flood hazard provoked direct impact on the population and/or infrastructures, in agreement with EM-DAT

definition. The inconsistency that sometimes exists between the databases with regards to representing the extent of the flood affected or impacted areas is identified as a limitation in this paper.

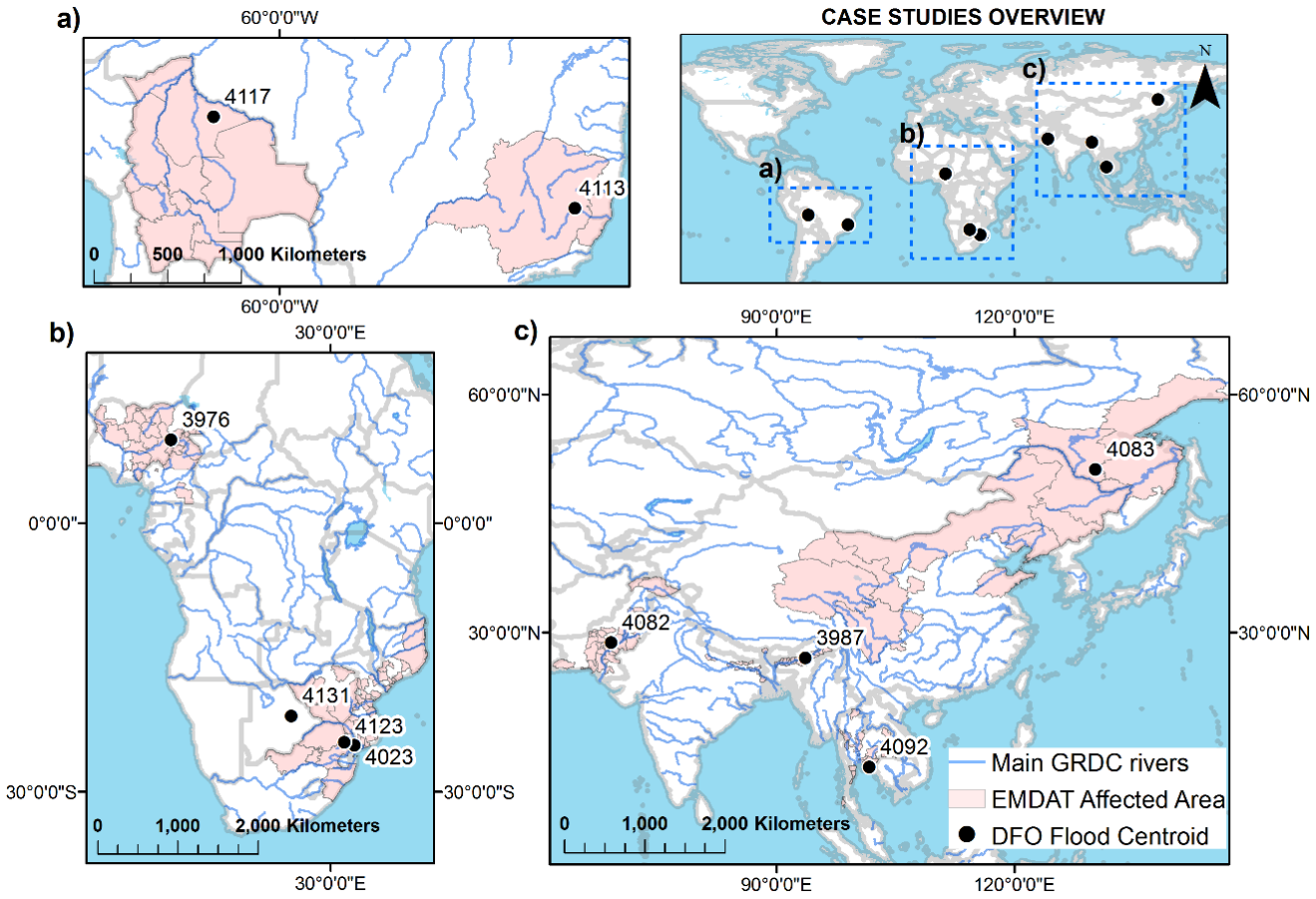

Figure 1. Location of the 10 flood events as recorded in the Dartmouth Flood Observatory with DFO centroid and Id number indicated. The flood-impacted regions from EM-DAT are shown as shaded polygons. Lines represent main GRDC Rivers (blue) and country borders (grey). Panels show (**a**) South America, (**b**) Africa, and (**c**) Asia.

Table 1. List of the 10 selected flood case studies from the Dartmouth Flood Observatory Archive [47]. The upstream areas of the DFO centroids were calculated from the local drainage map of GloFAS [4].

Case Study ID	DFO ID #	Country	Detailed Locations	Began	Ended	Cause	DFO Centroid X	DFO Centroid Y	Upstream Area (x1000 km^2)
1	3976	Nigeria, Cameroon	Adamawa state, eastern Nigeria, Kogi state	25/08/2012	26/09/2012	Heavy rain, Dam released	12.1089	9.30166	170
2	3987	India	Assam, north-eastern India	19/09/2012	15/10/2012	Monsoonal rain	93.6379	26.8031	469
3	4023	Mozambique, Namibia, Malawi, Zimbabwe	Limpopo river basin in southern province of Gaza, Zimbabwe along border with South Africa, KwaZulu-Natal in South Africa, northern Mozambique	17/01/2013	4/3/2013	Heavy rain	32.6773	−24.8006	329
4	4083	China, Russia	NE China, including Fushun City, Liaoning Province	7/8/2013	14/10/2013	Heavy rain	130.272	50.5323	914
5	4082	Pakistan	Punjab, Sindh, and Baluchistan	7/8/2013	21/08/2013	Monsoonal rain	69.1065	28.7404	742
6	4092	Thailand	26 of 77 provinces	30/09/2013	14/10/2013	Monsoonal rain	101.694	13.0819	1.2
7	4113	Brazil	Southeast states of Minas Gerais, and Espirito Santo	23/12/2013	04/01/2014	Heavy rain	−41.9423	−18.9538	81
8	4117	Bolivia	La Paz, Beni, Santa Cruz and Cochabamba; north-eastern Bolivia	10/1/2014	1/5/2014	Heavy rain	−64.0135	−13.3888	161
9	4123	Mozambique	Johannesburg, Kliptown, Soweto, eastern South Africa, Zimbabwe, and SE Mozambique, Kruger, Incomati River	24/02/2014	10/3/2014	Heavy rain	31.5459	−24.4459	54
10	4131	South Africa, Namibia, Botswana, Zimbabwe	SADC region, Zambezi River Limpopo, Mpumalanga, North West, Gauteng, KwaZulu Natal	1/3/2014	30/03/2014	Heavy rain	25.6074	−21.5153	223

2.2. Satellite-Derived Global Flood Monitoring

2.2.1. GFDS Flood Magnitude

The Global Flood Detection System (GFDS) [36] estimates the change in surface water extent based on signal information from satellite-based passive microwave sensors. This system uses the difference in brightness temperature, at a frequency of 36.5 GHz, between water and land surface to estimate the proportion of water within-pixel over land. To minimize the influence of cloud and local ground factors, the signal from the "wet pixel" within the river reach is normalized using a signal from a nearby "dry pixel" [14]. The ratio of the wet to dry pixels is produced daily at $0.09° \times 0.09°$ global grids. The GFDS also provides the anomaly of the flood signal estimated as the number of standard deviation from the long-term mean [14]. This anomaly, referred to as GFDS flood magnitude, has higher positive values (above the long-term mean) for large floods, and negative values (lower than long-term mean) for dry conditions. In this study, as in the currently operational GFDS, a four day forward-running mean of the GFDS flood magnitude is used in order to avoid any missing days [36] in the satellite data.

Depending on the termination and launch of different satellite missions, GFDS has used data from a combination of different passive microwave sensors since 1998, including the Tropical Rainfall Measuring Mission (TRMM, [51]), the Advanced Microwave Scanning Radiometer for Earth Observation System (AMSR-E, [52]),AMSR2 [53], and the Global Precipitation Measurement (GPM, [54]). For all selected flood events in this study, the GFDS flood signal and magnitudes were estimated based on passive microwave signal from TRMM and AMSR2, since AMSR-E was no longer active and GPM was not yet included during the period of interest, from August 2012 until May 2014.

2.2.2. MODIS Flood Maps

Flood maps were also derived from the satellite-based MODIS Near Real-Time Global Flood Mapping Project [39]. Global daily surface and floodwater maps from MODIS are produced at 250 m resolution, in $10° \times 10°$ global tiles. Onboard the National Aeronautic and Space Admiration (NASA)'s Terra and Aqua satellites, the MODIS instrument provides twice daily near-global coverage in two optical bands. The MODIS Water Product (MWP) is currently produced for each global land pixel with four assigned values ranging from 0 to 3, which correspond to an invalid data, a no water pixel, a reference pixel with water and a flood pixel respectively. Previous evaluation of the flood and permanent water detection of the MODIS Near Real-Time (NRT) Global Flood Mapping Product [39] indicated that the extreme terrain, terrain shadows, volcanic surface materials (young and un-vegetated lava flows), and cloud shadows are the main source of errors in flood detection. In this study, to minimize the effects of cloud and terrain shadows we use the MODIS Flood Map (pixels with a MWP value of 3) estimated based on composite of 2-day observation window (2D2OT, v.4.9) from both Aqua and Terra satellites.

2.2.3. GloFAS Flood Forecasting

Streamflow forecasts for the case studies were derived from the Global Flood Awareness System (GloFAS) [4], which is a scheme that generates medium-range daily ensemble streamflow forecasts and flood threshold exceedance probabilities for all rivers with upstream areas of more than 4000 km^2 worldwide at a 0.1 °grid resolution. The GloFAS uses a coupled land surface and distributed hydrologic model. The meteorological forcings are obtained from the Ensemble Prediction System (ENS) of the European Centre for Medium-range Weather Forecasting (ECMWF) [55]. The land surface energy and water balance calculations are performed by the Hydrologically modified Tiled ECMWF Scheme for Surface Exchanges over Land (H-TESSEL) [56,57]. Then, the surface and subsurface runoffs are routed along river channels using a one-dimensional LISFLOOD channel routing module [58,59] with a four-point implicit finite difference solution of the kinematic wave equation [60], accounting for flow routing and groundwater processes. For a full description of the model the reader is refer to [4,58,61]. For the selected flood events, we extracted 1- to 10-day lead forecasts and flood threshold exceedance probabilities from real-time GloFAS forecasts for the duration of the reported flood period. The reference climatology for determination of critical flood thresholds was derived based on ECMWF reforecasts, which are routinely produced using the most recent weather model [61].

3. Methods

We evaluated the skill of the satellite-based GFDS, the MODIS Flood Map, and the streamflow generated by the GloFAS model to monitor floods. This was done by investigating the spatial and temporal dynamics of all systems for the selected flood events. Due to the lack of publicly available *in situ* streamflow, or flood extent measurements for the case studies, simulated streamflow is the only viable option for obtaining an independent streamflow time series for the evaluation of the satellite-detected flood. The three data products we evaluate are, however, independent of each other, and the "ground truth" from the flood archives is also independent of any of the satellite systems.

The evaluation method is based primarily on three statistics obtained from the flood archives: flood period, map of impacted area, and centroid of the affected area. As stated in Section 2.1, the flood period (*i.e.*, the start and end date) and the centroid of the flood affected area was provided by the DFO, and the map of the flood impacted area was obtained from CRED. For each selected flood event, the evaluation consists of the assessment of the spatial location of the flood event detected from satellite sensors and forecasted with the model simulation, and the temporal dynamics within the impacted area.

3.1. Flood Maps

For each flood event, we created daily flood maps from the GFDS flood magnitude, MODIS Flood Map (MFM), and GloFAS flood forecasts for all the days during the reported flood period. Firstly, for GFDS we produced Boolean maps (1 for a flood and 0 for no flood) using the daily flood magnitude estimates for each $0.09° \times 0.09°$ pixel over the impacted area and vicinity. The Boolean maps were produced based on whether the magnitude exceeds the recommended threshold value of four (GFDS magnitude > 4) [36]. This means that pixels with smaller GFDS flood magnitudes (including small floods) were classified as non-floods in this study, to focus on larger floods. For MODIS we also created

Boolean flood maps based on whether the pixel indicated flood (MFM) or not. The Boolean flood maps were aggregated over all days during the reported flood to create the GFDS and MODIS maximum flood extent. Then, we compare the maximum flood extent detected by the GFDS and MFM over the case studies.

For GloFAS forecasts, we calculated the daily flood probability for each $0.1° \times 0.1°$ model pixel over the reported flood area. The flood probability (between 0% and 100%) for each pixel is calculated as the percentage of the 51-ensemble streamflow forecast exceeding a critical flood threshold, which has been estimated from long-term model runs using ECMWFs data. Then, for both GFDS and GloFAS, we determined the total number of flood days during the reported flood period based on the threshold exceedance of each pixel. Specifically, in case of GFDS the total number of flood days is a count of days for which the GFDS flood magnitude is greater than 4, and for GloFAS it is the days for which the ensemble median exceeds a given return level. In this study, we selected a 20-year return level as representative of large floods, but this exercise can be repeated for any other flood magnitude.

3.2. Flood Detection Indicator

In order to compare how the systems detected the temporal dynamics of the flood, we contrasted the detection rate time series of GFDS and GloFAS during the entire flood period. For this, we defined a flood detection indicator as follows. For GloFAS, the indicator for each day is defined as the percentage of river pixels with upstream area $\geq$ 5000 km^2 within the impacted area that indicated a threshold exceedance probability of at least 50% (*i.e.*, corresponding to the ensemble median), where the flood threshold was determined as 20-year return level. To estimate the flood detection indicator for the GFDS we used high resolution (1 km) global flood hazard maps [62] produced for different flood magnitudes using a combination of hydrologic and hydraulic models. The streamflow climatology was produced based on global atmospheric reanalysis dataset ERA-Interim [63] as input to the hydrologic model. Then the high magnitude streamflow (e.g., 10-year return flood) is mapped to flood inundation using the 2D hydraulic model CA2D [64]. The evaluation of the global flood hazard map shows a good agreement with satellite imagery [62]. We used a global flood hazard map corresponding to a 14-year magnitude flood to determine flood plains at the GFDS resolution (0.09 °), and then we estimated the flood detection indicator for the GFDS as the percentage of the flood plain pixels where the GFDS indicated large flood (GFDS magnitude > 4).

3.3. Data Agreement at Specific Locations

We also evaluated the GFDS flood detection and GloFAS forecast skills at selected locations within the impacted area. This helps understand how the temporal evolution of a flood event was captured by the detection and/or the forecasting systems, and how they compare. A pixel on main river channel (Table 1) close to the reported centroid of the DFO impacted area was selected for each event and time series of the GFDS flood magnitude, and GloFAS ensemble streamflow forecast were extracted. Then, the time series of the two systems were compared during the flood period. The MODIS Flood Map was excluded in this analysis because it only classifies a given pixel as flood or no flood without providing the magnitude of the flood.

In order to quantitatively measure the agreement between GFDS and GloFAS, we calculated the Pearson linear correlation coefficient (r) for each flood event as:

$$r = \frac{\sum_{i=1}^{n}(s_i - \mu_s)(Q_i - \mu_q)}{\sqrt{\sum_{i=1}^{n}(s_i - \mu_s)^2}\sqrt{\sum_{i=1}^{n}(Q_i - \mu_q)^2}} \quad (1)$$

where *s* is the GFDS magnitude for a given flood event, *Q* the mean of the GloFAS streamflow forecast, μ_s is the mean of *s*, and μ_q is the mean of *Q* and *n* is the duration (days) of a flood event. Since the GFDS data contains information only on variability and timing, but not on magnitude of the flows in volumetric streamflow units, other traditional metrics such as root mean square difference cannot be calculated.

4. Results

4.1. Comparison of the GFDS and MODIS Flood Maps

Figure 2 shows examples of the maximum flood extent maps estimated by aggregating the GFDS flood magnitude and MODIS Flood Map over the total duration of the floods as reported by the DFO. The maps show the satellite-based detection pixels that indicated flood on any given day (*i.e.*, at least one day) over the duration of the flood event. For reference, we also show the overlay of the impacted area as provided by the EM-DAT for each event. In general, both remote sensing products detected flooding along parts of the major rivers, but the flood inundation patterns of the sensors are different.

For example, the passive microwave-based GFDS detected flooding over larger areas for the 2012 Nigeria case (see also Table 1), while the MODIS showed inundations only along the main river channels. Larger areas were identified as flood inundated by GFDS compared to MODIS for the 2014 Bolivia flood. Fairly similar detection patterns were observed for some other cases such as the 2013 flood in northeastern China/Russia, and Pakistan. Conversely, MODIS detected flood over a larger area for the 2012 floods of Brahmaputra River in India (maps not shown are provided as a supplementary material).

For some of the cases (e.g., Brazil and southern Africa), both satellite-based products either detected flood in a small area or showed scattered floods across the area of interest. Clearly, this provides little flood indication to end users who rely on these products to draw the right conclusions for their aid management or decision-making. The different flood detection characteristics of the two products can be attributed to their different sensors and resolutions used for detecting the water surfaces. The GFDS flood product is based on passive microwave sensing of water surfaces, while the MODIS products use optical imagery that can potentially be affected by cloud cover leading to missed flood cases. However, the MODIS products have higher resolution (250 m) compared to the GFDS (0.90 °grids, ~10 km at the equator), which, in the absence of clouds, enables it capture finer details of the surface water change.

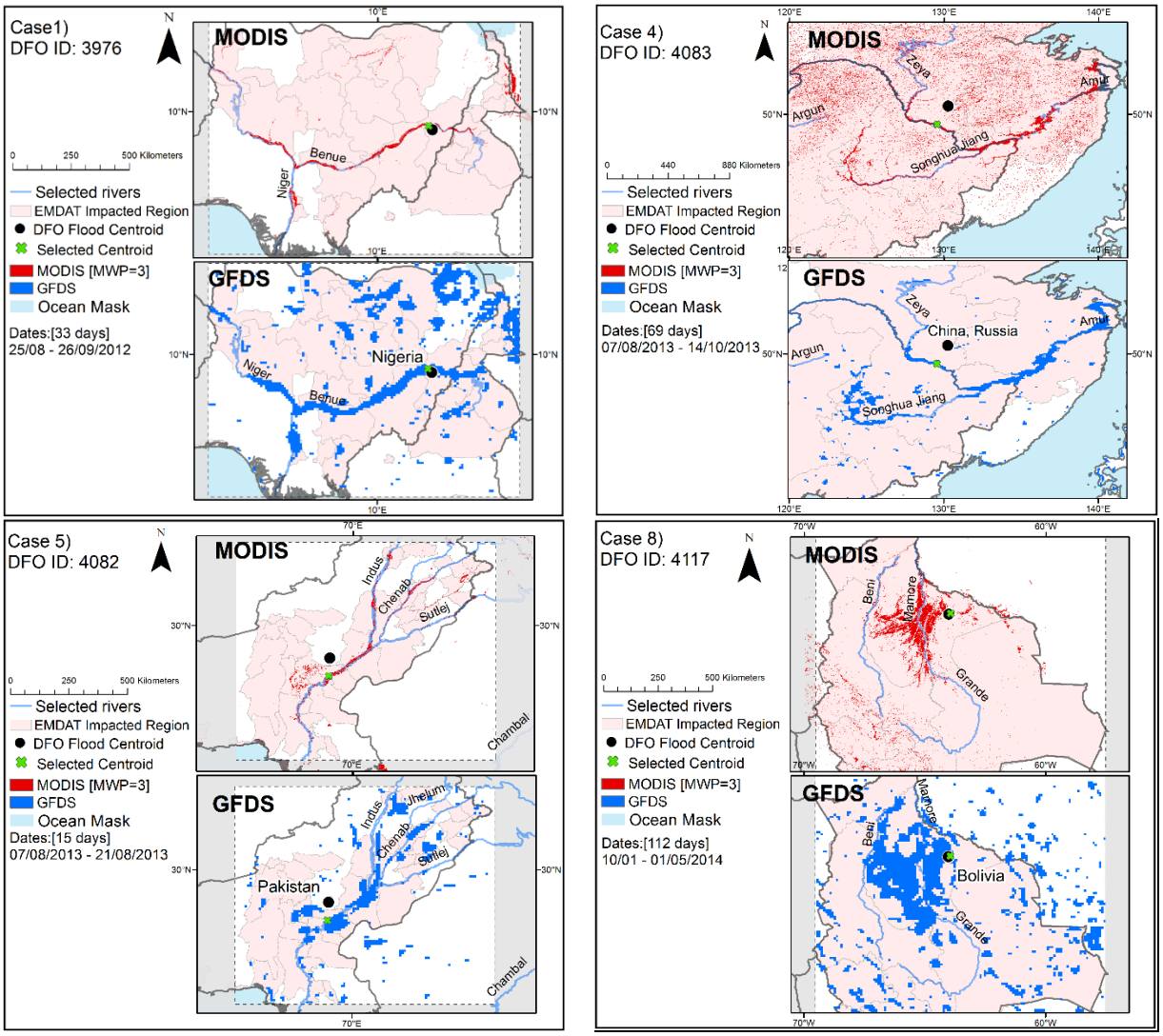

Figure 2. Maximum flood extent aggregated over the duration of a flood event as detected by GFDS (GFDS > 4) and MODIS Flood Map (MWP = 3). The flood cases shown are for Nigeria (2012), China (2012), Pakistan (2013) and Bolivia (2014).

4.2. Comparison of the GFDS and GloFAS

4.2.1. Flood Duration

Next we compare the GFDS flood magnitude detection and the GloFAS flood forecasts in terms of flood duration for the case studies. Figure 3 shows the percentage maps of days, from a total of the reported flood duration, when the detection or the forecasting systems indicated a flood event. Note that, on any given day and at a location, we determine that a flood has occurred for GFDS when the flood magnitude is greater than 4, and for GloFAS when the median of the ensemble forecast exceeds the 20-year flood threshold.

The flood map examples show the 2012 Nigeria flood (Case 1), the 2013 floods in China and Russia (Case 4) and in Pakistan (Case 5), and the 2014 flood in Bolivia (Case 8). The results indicate that the GFDS detected flooding over most parts of Benue River in the eastern Nigeria during the whole 33 days (100%) of the reported flood, while a long duration flood was also detected in parts of the lower reaches

of the Niger River. The floods detected over Benue River correspond well with the causes of the devastating flood of 2012 in Nigeria, which are heavy rainfall and the emergency release of water from Lagdo dam in upstream country Cameroon[65]

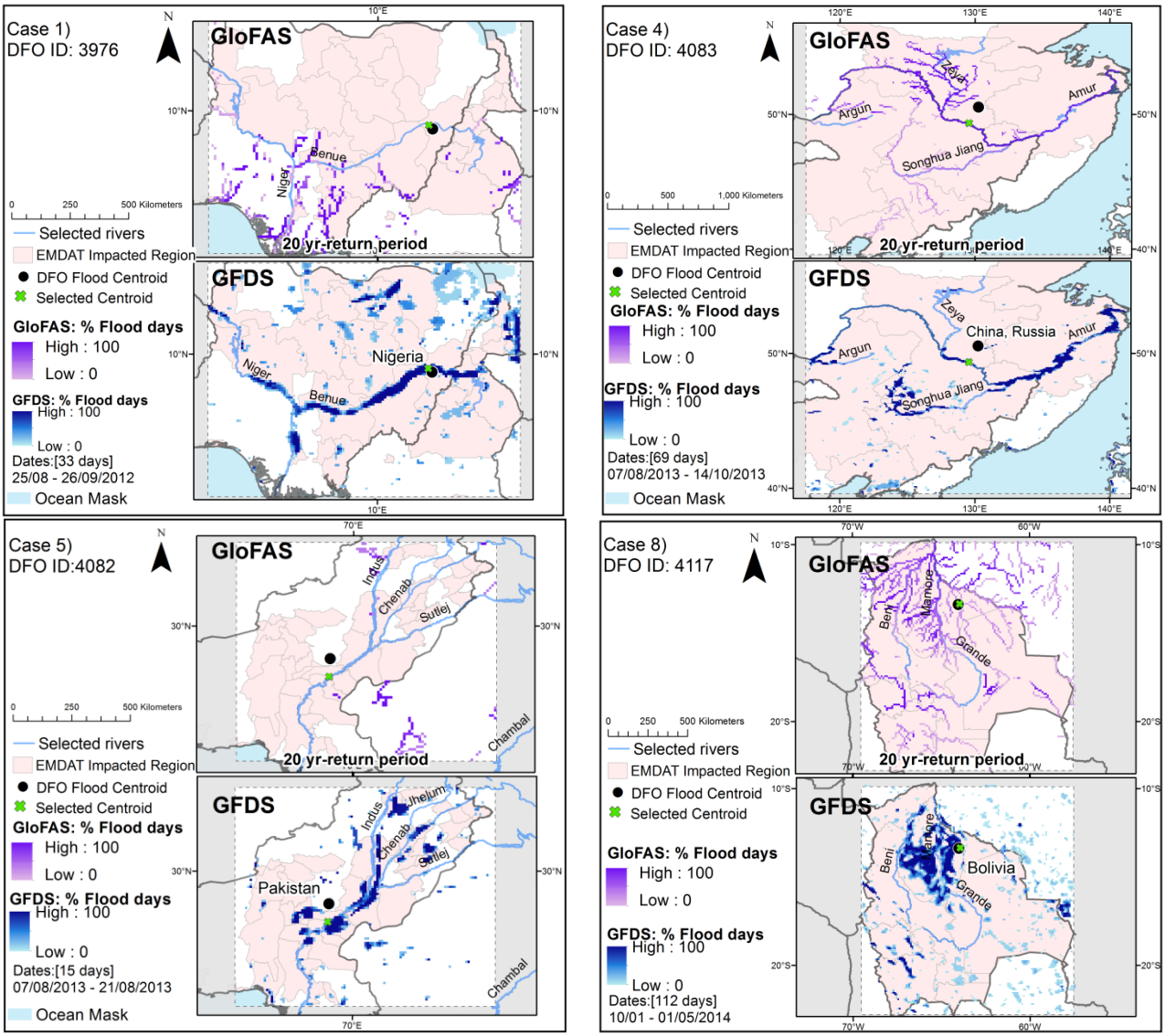

Figure 3. Total number of detected/forecasted (one-day lead for GloFAS) flood days expressed as the percentage of the total duration of flood. The flood cases shown are from Nigeria (2012), China and Russia (2013), Pakistan (2013), and Bolivia (2014).

In contrast, the flood on the upper Benue River (in both Cameroon and Nigeria) was not captured by the GloFAS forecast. There may be several reasons for this, one being the fact that flooding was intensified by the dam operation, and therefore, GloFAS (which does not take dam operations into account), was not able to capture the sudden increase of water in the river channel. Such processes can only be included when dam operations or real time inflow and outflow information is known. In the absence of *in situ* measurements or an established communication between the dam operators and GloFAS, remote sensing data could play an important role in improving the forecasting performance of such systems. The floods in downstream reaches of Benue and Niger Rivers were, however, picked up by the GloFAS forecast. These flood were forecasted to last for as long as the entire reported duration.

When other parts of the impacted area (from EM-DAT) were considered, the GloFAS forecast showed no major flood, while the GFDS detected some floods in the northern parts of the country.

The 2013 heavy flood of the Amur River in north-eastern China and parts of Russia, which lasted for 69 days, was partly detected by the GFDS. Particularly, flooded areas in the downstream reaches of the river were consistently observed by the microwave sensors. The GloFAS forecast showed high flows for the whole flood period in almost all parts of the Amur River. For the 2013 Indus River flooding in Pakistan, the GFDS detected floods for all days during the reported duration along some parts of the Indus River, while GloFAS forecasts similarly indicated high flows for upper reaches of the Indus and Chenab Rivers corresponding with the 20-year return period. The GloFAS failed to detect flood for the lower reaches of the Indus River when the 20-year flood threshold was used. Conversely, when a five-year threshold was used, the GloFAS detected flood in wider areas of the river basin (see supplementary material), suggesting that a lower flood magnitude (less than 20-year) may have occurred. The detection and forecasting systems were effective in measuring the 2014 Bolivian flood. The GFDS showed a vast area in the northern lowlands of the country between Beni and Mamore Rivers covered with water for almost all days from January to the end of April. There were also high streamflow forecasts from GloFAS for most of the lowland channels river during the majority of the reported flood period.

For the other case studies, varying characteristics of flood detection/forecasting were observed. The GFDS missed the 2012 flood in North Eastern India with detection only for a maximum of 40% of the reported days over parts of the Brahmaputra River, while GloFAS forecasted high streamflow for the majority of the days. Results for the 2013 floods in Thailand also indicated intermittent flood detection by the GFDS but high flows by the GloFAS, mainly exceeding the five-year return period. The December 2013 flooding in eastern Brazil was forecasted by GloFAS to only exceed the five-year return period, whereas the GFDS flood detection is highly scattered, probably due to low magnitude of the streamflow. The floods in Southern African Rivers were detected with mixed results. GloFAS forecasts showed the Zambezi floods of 2013 and 2014, as well as Okavango and Limpopo floods in 2014, while GFDS detection was irregular over distributed parts of the region.

The results shown in Figure 3 highlight the difficulties of using the output from anyone of the GloFAS and GFDS systems for decision-making. For example, in some cases floods are not captured during the entire duration of the flood over large parts of the impacted area, and can potentially make it difficult for humanitarian aid and civil protection organizations to act if decisions would be taken only based on these systems. A disagreement on a flood between the systems also could lead to a similar uncertain outcome. In addition, these systems provide information about flood hazard based on the anomalies of river streamflow or flood inundation, but they do not yet include other components of risk, such as exposure, vulnerability, and coping capacity to a disaster. This poses an additional challenge to disaster response organizations with respect to planning and resource allocations.

4.2.2. Flood Indicator Time Series

Figure 4 shows a time series of the flood detection indicator for the GFDS and GloFAS. This represents the total grids, as a percentage of the total grids that can potentially be flooded, where a flood is detected (or forecasted) on a given day. The potentially flooded grids were separately determined for both systems following the procedure described in Section 3.2. The results showed that the GFDS and

the GloFAS have different flood extent time-variations for different flood cases. For instance, in the case of the 2012 flood in Nigeria (see Figure 4, Case 1), the GFDS percentages of grids within the flood plain increased from 3% at the beginning of the flood event (25 August 2012) to 22% at the end (26 September 2012). However, GloFAS indicated flooding for only about 5% of the major river pixels throughout the duration of the event. Similarly the GFDS flood detection ratio was higher than for GloFAS for 2013 flood in Pakistan (Case 5) where the latter consistently indicated low extent.

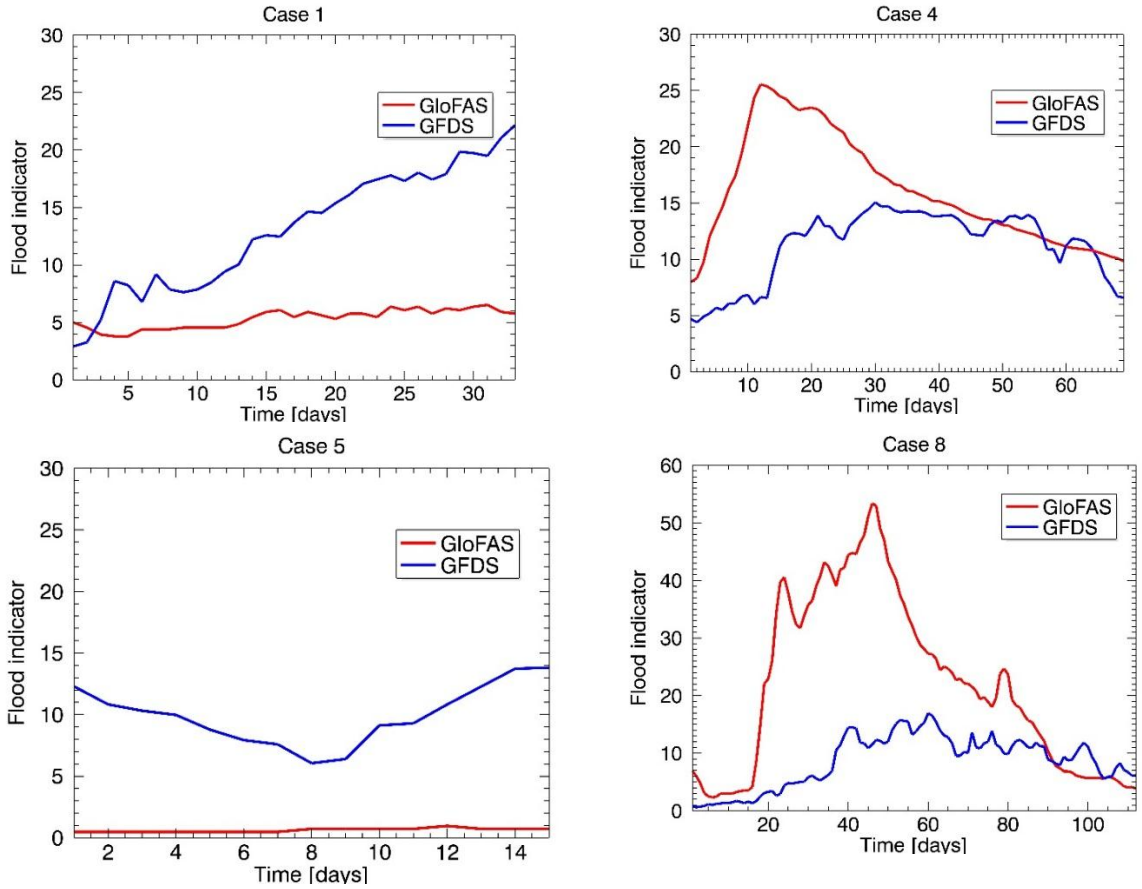

Figure 4. Time series comparison of the flood extent (% of grids indicating flood) for the GFDS detection (Magnitude > 4) and GloFAS 1-day lead forecast (median > 20-year flood). This represents the total observation (or model) grids, as a percentage of the total grids that can potentially be flooded (see Section 3.2). Note that the vertical axis is different for Bolivia (Case 8) due to the larger flooded areas and the horizontal axes are the days during the reported flood event.

Different dynamics was observed for the 2013 flood in the China-Russia border (Case 4): the GloFAS indicated increasing flood extent (up to 25% of the major river pixels) during the first 10 days, and recessing extent for the remaining. Meanwhile, GFDS also showed similar dynamics in terms of the flood extent rise at the beginning, and fall at the end of the event. However, the maximum flood extent in the latter case is significantly lower (15%). In a similar manner, GloFAS indicated a considerably larger flood extent than the GFDS for the 2014 Bolivian flood, and it was observed that the GFDS showed consistently lower flood extent for the 2012 flood in India (Case 2). In addition, for these three events, we can also see how there is a time lag between the GloFAS and the GFDS largest flooded areas.

In the case of the 2014 flood in Southern Africa (Case 3), the GFDS flood detection ratio was higher than for GloFAS, whereas for the flood events in Thailand (Case 6), Brazil (Case 7), Mozambique (Case 9) and Southern Africa (Case 10) the detection rate for both systems are low. We note that if a lower flood threshold (e.g., five-year level) is used instead of the 20-year level presented here, the GloFAS flood extent would considerably increase. Similarly for the GFDS, a lower threshold for flood magnitude (e.g., 2) would result in higher flood extent detection.

4.2.3. Onset and Evolution of the Flood Events

Figure 5 shows the time series of the GFDS flood magnitude and the 51-ensemble streamflow forecasts (five-day lead) from GloFAS, at selected locations (Table 1) on a major river network within the flood impacted areas. For each of the selected location, there is a fairly good agreement between GFDS and GloFAS time series, especially for the onset of the flood event for Cases 2, 3, 4, 5, 8 and 9, although in some cases there is few days of time-lag. The time-lag was also reported in previous study of by Revilla-Romero *et al.* (2014) [15], where they show that at many river locations there is a time-lag between the peak of the *in situ* streamflow and the peak of the inundation extent detected by GFDS.

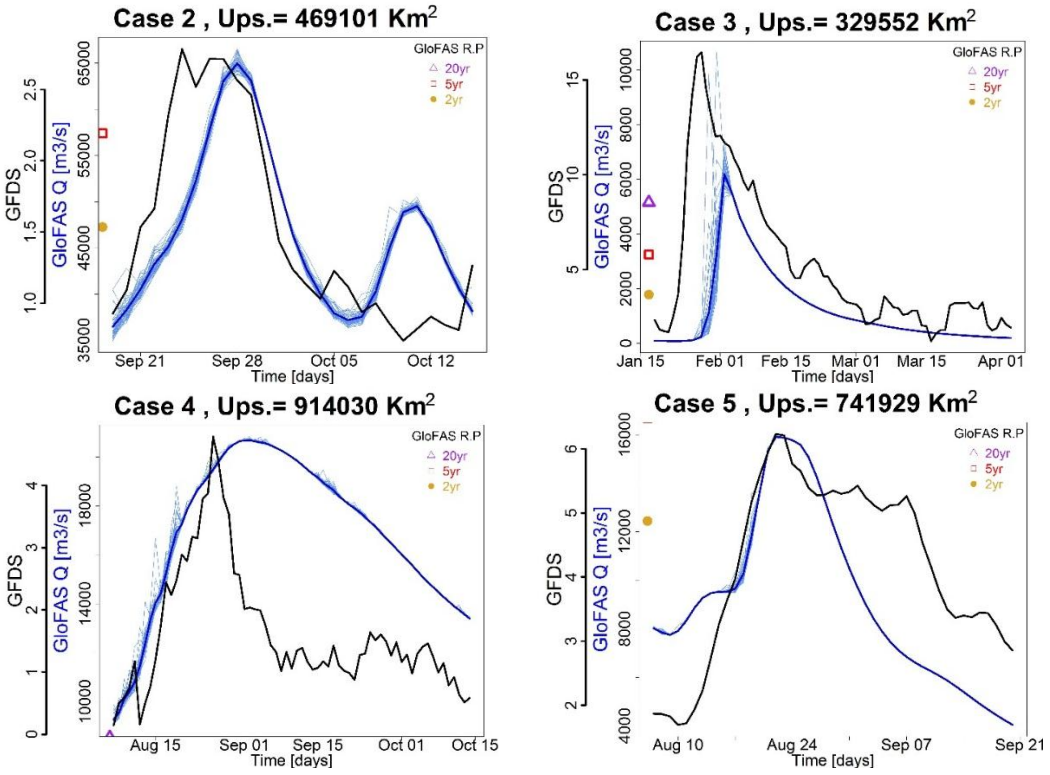

Figure 5. Time series of the probabilistic ensemble GloFAS forecast at five day lead-time [51] ensemble members (blue) and ensemble mean (dark blue), and the time series of the detected GFDS magnitude (black) during the days that the reported flood period by DFO. For information, the GloFAS upstream area is displayed for each location as well as the two-, five-, and 20-year return period.

For Case 1, in the upper Benue (Nigeria) the flood signal from GFDS is stronger, whereas GloFAS did not forecast extreme streamflow at that location, which may be explained by the human induced

intensification of the flood wave provoked by the sudden release of the water from an upstream dam as explained in Section 4.2.1. For Cases 6 and 9, the simulated flows indicate low values (< 200 m^3 s^{-1}) for which is it expected that the performance of the GFDS or GloFAS could be not reliable. In most of the cases, both GloFAS and GFDS captured flood at least for a few days during the time frame obtained from the DFO. However, for other cases (e.g., Cases 1, 5, 6 and 9) extended time periods was needed to capture the full length of the onset or the end of flood at that location. For example when the time series for Case 5 is extended by one month after the end of the reported end of the flood, then the falling limb of the flood peak is fully captured. Finally, GloFAS forecasts considerably exceeded 20-year return levels for some cases, but in other cases only two- or five-year return levels were exceeded. Furthermore, Pearson skill score was calculated between the GFDS magnitude and the mean of the GloFAS ensemble forecast (see Table 2). A high correlation was found for majority of the cases (> 0.50 for six and > 0.75 for four of the cases), while the correlation is low (< 0.4) for four of the flood events: Cases 1, 7, 8 and 10.

Table 2. Summary of the results from analysis of the GFDS and MODIS flood detection, and GloFAS forecast for the 10 case studies. *****Based on five-day lead GloFAS exceedance of the 20-year return level (for Case 5, a five-year return level is indicated).

Case Study	Forecasted *	GFDS Detected	MODIS Detected	Time Series. Captured	Correlation Time Series	Comments
1	Partially	Yes	Yes	Yes if extended	0.33	GFDS capture flood in Benue river due to water released from dam in Cameroon, while GloFAS not fully forecasted the intensity of the event, aggravated by the release of the water from the dam. Longer reported date needed to fully capture the event. DFO centroid within the impacted area.
2	Yes	Partially	Yes	Yes	0.78	Flood extent match, but not very strong signal in GFDS along all the Brahmaputra. DFO centroid within the impacted area.
3	Yes	Yes	Partially	Yes	0.86	Agreement mainly on the Limpopo and Zambezi rivers. Larger floods were detected and forecasted further upstream. DFO centroid within the impacted area.
4	Yes	Yes	Yes	Yes	0.54	Flood extent match in main Argun, Songhua Jiang and Amur river, but with disagreement in Zeya. DFO centroid within the impacted area, but it is far from main river.
5	Partially (5 yr-return level)	Yes	Yes	Yes if extended	0.61	Flood extent match in main Indus and Chenab rivers. Extended dates were needed to fully capture the event. DFO centroid outside impacted area, and far from main river.

Table 2. *Cont.*

Case Study	Forecasted *	GFDS Detected	MODIS Detected	Time Series. Captured	Correlation Time Series	Comments
6	Yes	Yes	Yes	Yes if extended	0.82	Flood extent match, noise in GFDS signal due to proximity to coast. Extended dates needed to fully capture the event. DFO centroid within the impacted area
7	Partially	Scattered	No	No	−0.2	Scatter flooded area in GFDS and there was no MFM detection. DFO centroid within the impacted area.
8	Yes	Yes	Yes	Yes	0.35	Clear flooded extent was observed in Beni and Grande rivers. DFO centroid within the impacted area.
9	No	Scattered	Scattered	Yes if extended	0.84	GloFAS forecasted for Limpopo, Zambezi and Shire rivers. Scattered GFDS flood extent was observed, and do not match impacted area. There was no MFP detection. Extended dates are needed to fully capture the event. DFO centroid outside the impacted area, and far from main river.
10	Partially	Scattered	Scattered	Yes	0.12	There is spatial disagreement, especially in Namibia and Botswana. Namibia flooded extent matched with the Great Escarpment area and is during the rainy season. There is noise in GFDS signal due to proximity to coast. No MWP detection. DFO centroid outside the impacted area, and far from main river.

5. Discussion

Global remotely-sensed information such as flood magnitude, timing, and spatial extent can play a key role for decision makers when a flood disaster strikes, especially in areas with limited accessibility of *in situ* data. This information can be complemented with flood forecasting models or used for validation of independent international databases. Several studies have evaluated the quality of remote-sensing products from optical imagery (e.g., MODIS, ASTER and Landsat TM/ETM+), or passive microwave (AMSR-E) by comparing them with each other or with other datasets like streamflow time series, flood damage curves [37,40–43], or model simulated stream flows [44,45]. However, the quality of the operationally used flood maps from MODIS and GFDS, and the flood forecasts from GloFAS, as performed in this study, were not previously evaluated at a global scale.

The overall summary of the performance of the detection and forecasting systems for the ten case studies are presented in Table 2. The spatial and temporal characteristics of the flood detected by each system vary for different flood cases. The strengths of each of the individual systems and their

independence make them complementary and useful tools for robust global flood disaster management. However, there are several limitations in each individual system that should be taken into consideration.

5.1. Known Limitations

We comparatively evaluated three global systems for correctly detecting flood events using 10 case studies. The case studies were selected from the global flood archives where only qualitative flood magnitude is provided. The DFO archives (a primary source of flood events in this study) were created primarily based on several news reports, which makes it difficult to verify the accuracy of the flood information. For example, the centroid of the affected area, and the start and end dates of the flood are among the key flood parameters used in the evaluation of the detection and forecasting systems. They are also used to evaluate the impacts post-event, and if not accurately estimated, that can lead to missing the location and timing of a flood event. The area impacted by flooding from EM-DAT is generally overestimated due to the use of full administrative units (e.g., GAUL Level 1), and a more detailed maps (e.g., GAUL Level 2) were not always available on the disaster reports provided by EM-DAT.

The satellite-based flood detection systems also have their limitations. The MODIS Water Product is derived from optical imagery, which has known problems with cloud cover and terrain shadows. The effect of the terrain shadow is removed using a masking algorithm in the data used in this study (2D2OT, v4.9) but the problem of cloud cover results in some floods remaining undetected. The GFDS flood magnitude estimates are produced at higher spatial resolution ($0.09° \times 0.09°$), which lumps larger area all together and is only suitable for large-scale floods. Moreover, passive-microwave signal detection varies mainly depending on the river profile [66], but also by local conditions at those locations affected by flooding [15,67]. Besides, the uniformly selected threshold of 4 for the GFDS flood magnitude in all 10 case studies may be too high, and in some cases a magnitude of 2 could possibly mean a large flood.

The GloFAS forecasts could be influenced by several factors such as uncertainties in meteorological forcing, hydrological model, and initial conditions, and man-made factors, which are not accounted for by the model. The hydrologic model used for producing the streamflow forecast is not calibrated, and lake (and reservoirs) modules are not included of the model setup evaluated in this study. Furthermore, we selected the 20-year flood threshold for determining the occurrence of large floods, which could potentially lead to low detection rates. Lower thresholds could be tested, and more analysis could be performed using different forecast lead-times (e.g., 1–10-day). It is also evident that the GloFAS forecasts are streamflow magnitudes, and do not indicate the flood inundated area which makes it difficult to directly compare with the satellite-based flood maps.

Moreover, small-scale floods (short duration and smaller spatial extent) are currently more difficult to capture by the satellite sensors and the hydrologic model mainly due to the coarse resolutions at which these systems operate. The GloFAS and GFDS systems have been designed to currently operate at ~10 ° spatial resolution and daily time steps. A better global-scale detection and forecasting of small scale floods, however, could be possible in the future with improved remote sensing datasets (e.g., more frequent revisit time) and using a modeling approach suitable for such floods. Within GloFAS, there are current efforts focusing on the development of a global flash flood indicator, based on previous research and experiences gained from the flash flood indexes currently operational within the European Flood Awareness System (EFAS), such as the European Precipitation Index based on Climatology (EPIC) [68]

and European Runoff Index based on Climatology (ERIC) [69]. Outside these systems, extensive international efforts are being put to set up a global operational flash flood warning system [70].

5.2. Implications for Decision Makers

The GloFAS, GFDS, and MODIS NRT systems are automated, presently pre-operated with reliable plans for continuity, and already being used by some decision makers or related entities (including International Red Cross/Red Crescent, World Food Program, the World Bank, the Latin American Development Bank, and others). While they represent novel and quite different capabilities than have been available in the past, much experience is still to be gained in their practical implementations. The flood forecasting and detection systems provide the flood hazard with regards to the intensity, location, and timing of a given flood disaster. Despite the uncertainties and their known limitations, these systems have already been used for humanitarian responders [8,9,38] especially in regions with limited flood forecasting and riverine monitoring systems.

It should be emphasized, however, that the end-users must be aware of the skills, suitability and limitations of these systems before taking decisions based on the outputs of these systems. In some of the flood cases considered in this study, the forecasting system failed to capture at any or parts of a river reaches, while in other cases the satellite-based detection systems similarly missed. This suggest that the decision makers should utilize all available forecast and detection resources before taking any action, instead of relying solely on one system, for reaching an optimal decision. This is particularly important due to the fact that each system provides a unique and pivotal piece in flood monitoring apparatus. The forecasting systems help the decision maker oversee upcoming disaster before it occurs, while the real-time detection systems provide data about an ongoing disaster. Another important issue that may be of interest to the decision makers is the continuity of the flood forecasting and detection services. For instance, the remote sensing products (e.g., GFDS) rely on the launch and termination of satellite missions. Furthermore, some research products may provide no guarantee to continue providing flood services beyond the end of the research project. While the systems presented in this study are expected to continue providing the services for the foreseeable future, decision makers should be generally aware of the lifespan of any operational system and limit a complete dependency on a short-lived system.

The forecast lead-time needed by the disaster response organizations to take preparedness actions varies. For example, a few days might be enough for civil protection, and for humanitarian organizations such as Red Cross/Red Crescent and World Food Program to deploy resources, while a farmer will need longer lead-times in order to secure its cattle or crops. In previous disasters, *a posteriori* analysis showed that if humanitarian responders start to act when the (flood) hazard is already happening, this will generally derive the costs higher and causes more damage to the communities than if they are aware and ready to act before the disaster strikes. Although, standardized ground information on the location, timing and impacts [49] for each event is needed in order to fully be aware of where flooding really took place and where the biggest impacts.

Evidently, the flood hazard forecast alone is not sufficient to fully understand the disaster impact and take actions. There are efforts to develop global flood risk models [71] that takes into account all components of flood risk: hazard, exposure, and vulnerability. Additionally, an Index for Risk Management (INFORM), a humanitarian risk index [72] designed to support decisions about disaster

prevention, preparedness and response, incorporates the coping capability to disaster risk assessments. The global flood forecasting and detection systems evaluated in this study are important pillars for building the flood risk assessment models and services.

6. Conclusions and Future Research Direction

In this study, we evaluated satellite-based flood detection and model-based forecasting systems using 10 riverine flood case studies located in Asia, Africa, and South America. We assessed remote-sensing data from the Global Flood Detection System (GFDS) and MODIS Flood Map (MFM), and ensemble streamflow forecasts from the Global Flood Awareness System (GloFAS) using flood information obtained from global flood disaster databases such as the Dartmouth Flood Observatory (DFO) Archive and the EM-DAT database. The main conclusions of the study are as follows:

(1) Quantitative validation of the different global models in data sparse regions is difficult due to the vast difference in the characteristics of the reference datasets from remote sensing and the lack of ground-based streamflow measurements. However, we performed a series of objective tests, and have provided some numerical assessments of detection and measurement accuracy.

(2) General agreement was found between GFDS, MODIS and GloFAS for large floods. However, large differences exist in the spatio-temporal characteristics of the flood detections as recorded, simulated, or monitored by the different systems. All three automated flood prediction/detection/monitoring systems would provide early notice and useful independent characterization information for each major flood.

(3) Each system has its limitations, which should be understood before using them for operational flood monitoring. The spatial resolution that systems operate in must always be considered (e.g., the remote sensing methods are not useful for flash floods in narrow mountain valleys). Cloud cover obscuration from the MODIS system cannot be avoided. However, the microwave technology is not so affected, so may provide early warning at low spatial resolution with MODIS then providing more detailed mapping as cloud cover parts. Future improvements of the global models and satellite missions coming up (and improved retrieval algorithms) specifically designed, for example, to derive water levels or river widths [66,67] may significantly address these limitations.

However, more work is necessary for fully utilizing the flood forecasting and detection systems for decision-making. Firstly, in order to ease the verification of the global remote sensing and hydrological/hydraulic model outputs, the solution would be to increase the station density network of gauging stations [10]. However, as this is unlikely to happen, the scientific community has been exploring other possible solutions, and a large part of this effort is focusing on the use of remote sensing data [73]. Recent and future satellite missions have been specifically designed for measuring water levels or river widths from satellite imagery [74–76], which can be used to derived river flows. The Surface Water & Ocean Topography (SWOT) mission with its wide-swath altimetry technology will contribute to further the understanding of the surface water part of the global water cycle. Further, there has been improvements in radar and optical imagery for flood extent mapping such as COPERNICUS rapid mapping using the European Space Agency SENTINEL-1 SAR mission, at a resolution of 10 meters, and other satellites such

as Landsat-8 with a resample pixel size of 30 meters that is used in this context to map pre-flood water extent (for an example, see Pakistan Floods (July 2015) [77].

Other ways forward within the GFDS data could be the use of higher resolution data for this product, "cleanup" of GFDS flood signal using the global flood hazard map [62] derived from GloFAS in order to focus on large riverine floods, to study how the effect of the four different sensors (TRRM, AMSR-E, AMSR2, GPM) used during the life time of the GFDS product since 1998 affected the long-term data quality and derivation of the Flood Magnitude product, and further validation research to establish the reason behind false flood signal. Furthermore, to improve global flood forecasting models, there is a need among other features to enhance the representation of hydrological processes, advance on the communication of uncertainty of the model outputs to the users, carry out model calibration, and test the effects of data assimilation such as remote-sensed soil moisture [20,21,78] and surface water extent, or levels [23] within hydrological models.

Additionally, in order to help to validate the output from global flood monitoring and forecasting systems, it will be useful from the Dartmouth Flood Observatory database if the flood centroid or the coordinates of an additional position is provided that is located within a river, in the case of riverine floods, rather than a flood centroid in occasions far from streams. More work could be done by the Flood Observatory of the Global Flood Partnership [3] to enhance the flood records and include more information such as flood disaster exposure, and vulnerability and coping capacity. Additionally, the post disaster impacted areas could be created based on a more detailed spatial scale (e.g., GAUL Level 2) to improve the accuracy of the affected areas.

Supplementary Materials

Figure S1: Same as Figure 2 but for Cases 2, 3, 6, 7, 9, and 10.
Figure S2: Same as Figure 3 but for Cases 2, 3, 6, 7, 9, and 10.
Figure S3: Same as Figure 4 but for Cases 2, 3, 6, 7, 9, and 10.
Figure S4: Same as Figure 5 but for Cases 1, 6, 7, 8, 9, and 10.
Figure S5: Same as Figure 5 but for Case 5, and 5-year return period.

Acknowledgments

We greatly thank Pascaline Wallemacq from CRED for providing us the geo-reference of the flood affected areas used in this study. The first author also thanks Ad de Roo for PhD supervision. The paper has greatly benefited from insightful comments of five anonymous reviewers.

Author Contributions

Beatriz Revilla-Romero and Feyera A. Hirpa designed the research framework, performed research, and analyzed the data and wrote the paper. As first author, Beatriz Revilla-Romero took the leadership behind this project, wrote most of the paper, and designed the graphs. Jutta Thielen-del Pozo sparked the idea behind this work. Jutta Thielen-del Pozo, Peter Salamon, Robert Brakenridge, Florian Pappenberger, and Tom De Groeve contributed in writing parts of the manuscript and helped editing it. All authors have read and approved the final manuscript.

Conflicts of Interest

The authors declare no conflict of interest.

References

1. Centre for Research on the Epidemiology of Disasters (CRED). The Human Cost of Natural Disasters 2015: A Global Perspective. Available online: http://reliefweb.int/report/world/human-cost-natural-disasters-2015-global-perspective (accessed on 25 August 2015).
2. Making Development Sustainable: The Future of Disaster Risk Management. Available online: http://www.preventionweb.net/english/hyogo/gar/2015/en/gar-pdf/GAR2015_EN.pdf (accessed on 25 August 2015).
3. De Groeve, T.; Thielen, J.; Brakenridge, R.; Adler, R.; Alfieri, L.; Kull, D.; Lindsay, F.; Imperiali, O.; Pappenberger, F.; Rudari, R.; *et al*. Joining forces in a global flood partnership. *Bull. Am. Meteorol. Soc.* **2014**, doi:10.1175/BAMS-D-14-00147.1.
4. Alfieri, L.; Burek, P.; Dutra, E.; Krzeminski, B.; Muraro, D.; Thielen, J.; Pappenberger, F. GloFAS—Global ensemble streamflow forecasting and flood early warning. *Hydrol. Earth Syst. Sci.* **2013**, *17*, 1161–1175.
5. Van Beek, L.P.H.; Bierkens, M.F.P. The Global Hydrological Model PCR-GLOBWB: Conceptualization, Parameterization and Verification. Available online: http://vanbeek.geo.uu.nl/suppinfo/vanbeekbierkens2009.pdf (accessed on 25 August 2015).
6. Yamazaki, D.; Kanae, S.; Kim, H.; Oki, T. A physically based description of floodplain inundation dynamics in a global river routing model. *Water Resour. Res.* **2011**, doi:10.1029/2010WR009726.
7. Wu, H.; Adler, R.F.; Tian, Y.; Huffman, G.J.; Li, H.; Wang, J. Real-time global flood estimation using satellite-based precipitation and a coupled land surface and routing model. *Water Resour. Res.* **2014**, *50*, 2693–2717.
8. Stephens, E.; Coughlan de Perez, E.; Kruczkiewicz, A.; Boyd, E.; Suarez, P. Forescast-Based Action. A Co-Produced Research Roadmap for Forecast-Based Pre-Emptive Action. Available online: http://www.climatecentre.org/downloads/files/Stephens%20et%20al.%20Forecast-based%20Action%20SHEAR%20Final%20Report.pdf (accessed on 25 August 2015).
9. Coughlan de Perez, E.; van den Hurk, B.; van Aalst, M.K.; Jongman, B.; Klose, T.; Suarez, P. Forecast-based financing: An approach for catalyzing humanitarian action based on extreme weather and climate forecasts. *Nat. Hazards Earth Syst. Sci.* **2015**, *15*, 895–904.
10. Hannah, D.M.; Demuth, S.; van Lanen, H.A.J.; Looser, U.; Prudhomme, C.; Rees, G.; Stahl, K.; Tallaksen, L.M. Large-scale river flow archives: importance, current status and future needs. *Hydrol. Process.* **2011**, *25*, 1191–1200.
11. Global Runoff Data Centre (GRDC). The River Discharge Time Series, Koblenz, Germany: Federal Institute of Hydrology (BfG). Available online: http://grdc.bafg.de (accessed on 25 August 2015).
12. Schumann, G.; Bates, P.D.; Horritt, M.S.; Matgen, P.; Pappenberger, F. Progress in integration of remote sensing-derived flood extent and stage data and hydraulic models. *Rev. Geophys.* **2009**, doi:10.1029/2008RG000274.

13. Smith, L.C. Satellite remote sensing of river inundation area, stage, and discharge: A review. *Hydrol. Process.* **1997**, *11*, 1427–1439.
14. Brakenridge, G.R.; Nghiem, S.V.; Anderson, E.; Mic, R. Orbital microwave measurement of river discharge and ice status. *Water Resour. Res.* **2007**, doi:10.1029/2006WR005238.
15. Revilla-Romero, B.; Thielen, J.; Salamon, P.; de Groeve, T.; Brakenridge, G.R. Evaluation of the satellite-based global flood detection system for measuring river discharge: Influence of local factors. *Hydrol. Earth Syst. Sci.* **2014**, *18*, 4467–4484.
16. Tarpanelli, A.; Brocca, L.; Lacava, T.; Melone, F.; Moramarco, T.; Faruolo, M.; Pergola, N.; Tramutoli, V. Toward the estimation of river discharge variations using MODIS data in ungauged basins. *Remote Sens. Environ.* **2013**, *136*, 47–55.
17. Gleason, C.J.; Smith, L.C. Toward global mapping of river discharge using satellite images and at-many-stations hydraulic geometry. *Proc. Natl. Acad. Sci.* **2014**, *111*, 4788–4791.
18. Birkinshaw, S.J.; Moore, P.; Kilsby, C.G.; O'Donnell, G.M.; Hardy, A.J.; Berry, P.A.M. Daily discharge estimation at ungauged river sites using remote sensing. *Hydrol. Process.* **2014**, *28*, 1043–1054.
19. Revilla-Romero, B.; Beck, H.E.; Burek, P.; Salamon, P.; de Roo, A.; Thielen, J. Filling the gaps: Calibrating a rainfall-runoff model using satellite-derived surface water extent. *Remote Sens. Environ.* **2015**, *171*, 118–131.
20. Wanders, N.; Karssenberg, D.; de Roo, A.; de Jong, S.M.; Bierkens, M.F.P. The suitability of remotely sensed soil moisture for improving operational flood forecasting. *Hydrol. Earth Syst. Sci.* **2014**, *18*, 2343–2357.
21. Hirpa, F.A.; Gebremichael, M.; Hopson, T.M.; Wojick, R.; Lee, H. Assimilation of satellite soil moisture retrievals into a hydrologic model for improving river discharge. In *Remote Sensing of the Terrestrial Water Cycle*; Lakshmi, V.; Alsdorf, D.; Anderson, M.; Biancamaria, S.; Cosh, M.; Entin, J.; Huffman, G.; Kustas, W.; van Oevelen, P.; Painter, T.; Parajka, J.; Rodell, T.; Rüdiger, C., Eds.; John Wiley & Sons Inc: Hoboken, NJ, USA, 2014; pp. 319–329.
22. Hostache, R.; Matgen, P.; Schumann, G.; Puech, C.; Hoffmann, L.; Pfister, L. Water level estimation and reduction of hydraulic model calibration uncertainties using satellite SAR images of floods. *IEEE Trans. Geosci. Remote Sens.* **2009**, *47*, 431–441.
23. Giustarini, L.; Matgen, P.; Hostache, R.; Montanari, M.; Plaza, D.; Pauwels, V.R.N.; de Lannoy, G.J.M.; de Keyser, R.; Pfister, L.; Hoffmann, L.; *et al*. Assimilating SAR-derived water level data into a hydraulic model: A case study. *Hydrol. Earth Syst. Sci.* **2011**, *15*, 2349–2365.
24. Di Baldassarre, G.; Schumann, G.; Bates, P.D. A technique for the calibration of hydraulic models using uncertain satellite observations of flood extent. *J. Hydrol.* **2009**, *367*, 276–282.
25. Domeneghetti, A.; Tarpanelli, A.; Brocca, L.; Barbetta, S.; Moramarco, T.; Castellarin, A.; Brath, A. The use of remote sensing-derived water surface data for hydraulic model calibration. *Remote Sens. Environ.* **2014**, *149*, 130–141.
26. Dung, N.V.; Merz, B.; Bárdossy, A.; Thang, T.D.; Apel, H. Multi-objective automatic calibration of hydrodynamic models utilizing inundation maps and gauge data. *Hydrol. Earth Syst. Sci.* **2011**, *15*, 1339–1354.

27. Sun, W.; Ishidaira, H.; Bastola, S. Towards improving river discharge estimation in ungauged basins: Calibration of rainfall-runoff models based on satellite observations of river flow width at basin outlet. *Hydrol. Earth Syst. Sci.* **2010**, *14*, 2011–2022.
28. Kundu, S.; Aggarwal, S.P.; Kingma, N.; Mondal, A.; Khare, D. Flood monitoring using microwave remote sensing in a part of Nuna river basin, Odisha, India. *Nat. Hazards* **2015**, *76*, 123–138.
29. Schumann, G.J.P.; Moller, D.K. Microwave remote sensing of flood inundation. *Phys. Chem. Earth* **2015**, doi:10.1016/j.pce.2015.05.002.
30. Birkett, C.M.; Mertes, L.A.K.; Dunne, T.; Costa, M.H.; Jasinski, M.J. Surface water dynamics in the Amazon Basin: Application of satellite radar altimetry. *J. Geophys. Res.* **2002**, doi:10.1029/2001JD000609.
31. Getirana, A.C.V. Integrating spatial altimetry data into the automatic calibration of hydrological models. *J. Hydrol.* **2010**, *387*, 244–255.
32. Sun, W.; Ishidaira, H.; Bastola, S. Calibration of hydrological models in ungauged basins based on satellite radar altimetry observations of river water level. *Hydrol. Process.* **2012**, *26*, 3524–3537.
33. Allen, G.H.; Pavelsky, T.M. Patterns of river width and surface area revealed by the satellite-derived North American River Width data set. *Geophys. Res. Lett.* **2015**, *42*, 395–402.
34. Durand, M.; Andreadis, K.M.; Alsdorf, D.E.; Lettenmaier, D.P.; Moller, D.; Wilson, M. Estimation of bathymetric depth and slope from data assimilation of swath altimetry into a hydrodynamic model. *Geophys. Res. Lett.* **2008**, doi:10.1029/2008GL034150.
35. Callow, J.N.; Boggs, G.S. Studying reach-scale spatial hydrology in ungauged catchments. *J. Hydrol.* **2013**, *496*, 31–46.
36. Kugler, Z.; de Groeve, T. *The Global Flood Detection System*; Office for Official Publications of the European Communities: Seat, Luxembourg, 2007.
37. Khan, S.I.; Hong, Y.; Gourley, J.J.; Khattak, M.U.; de Groeve, T. Multi-sensor imaging and space-ground cross-validation for 2010 flood along Indus River, Pakistan. *Remote Sens.* **2014**, *6*, 2393–2407.
38. Jongman, B.; Wagemaker, J.; Revilla-Romero, B.; Coughlan de Perez, E. Early flood detection for rapid humanitarian response: Harnessing big data from near real-time satellite and twitter signals. *ISPRS Int. J. Geo-Inf.* **2015**, *4*, 2246–2266.
39. Nigro, J.; Slayback, D.; Policelli, F.; Brakenridge, G.R. NASA/DFO MODIS Near Real-Time (NRT) Global Flood Mapping Product Evaluation of Flood and Permanent Water Detection. Available online: http://oas.gsfc.nasa.gov/floodmap/documents/NASAGlobalNRTEvaluation Summary_v4.pdf (accessed on 25 August 2015).
40. Brakenridge, R.; Anderson, E. Modis-based flood detection, mapping and measurement: The potential for operational hydrological applications. In *Transboundary Floods: Reducing Risks Through Flood Management*; Marsalek, J., Stancalie, G., Balint, G., Eds.; Springer Netherlands: Dordrecht, The Netherlands, 2006; pp. 1–12.
41. Memon, A.A.; Muhammad, S.; Rahman, S.; Haq, M. Flood monitoring and damage assessment using water indices: A case study of Pakistan flood-2012. *Egypt. J. Remote Sens. Space Sci.* **2015**, *18*, 99–106.

42. Huang, C.; Chen, Y.; Wu, J. Mapping spatio-temporal flood inundation dynamics at large riverbasin scale using time-series flow data and MODIS imagery. *Int. J. Appl. Earth Obs. Geoinf.* **2014**, *26*, 350–362.
43. Sakamoto, T.; Van Nguyen, N.; Kotera, A.; Ohno, H.; Ishitsuka, N.; Yokozawa, M. Detecting temporal changes in the extent of annual flooding within the Cambodia and the Vietnamese Mekong Delta from MODIS time-series imagery. *Remote Sens. Environ.* **2007**, *109*, 295–313.
44. Brakenridge, R.G.; Cohen, S.; Kettner, A.J.; De Groeve, T.; Nghiem, S.V.; Syvitski, J.P.M.; Fekete, B.M. Calibration of satellite measurements of river discharge using a global hydrology model. *J. Hydrol.* **2012**, *475*, 123–136.
45. Khan, S.I.; Hong, Y.; Wang, J.; Yilmaz, K.K.; Gourley, J.J.; Adler, R.F.; Brakenridge, G.R.; Policell, F.; Habib, S.; Irwin, D. Satellite remote sensing and hydrologic modeling for flood inundation mapping in Lake Victoria Basin: Implications for hydrologic prediction in ungauged basins. *IEEE Trans. Geosci. Remote Sens.* **2011**, *49*, 85–95.
46. Chapman, B.; McDonald, K.; Shimada, M.; Rosenqvist, A.; Schroeder, R.; Hess, L. Mapping regional inundation with spaceborne L-Band SAR. *Remote Sens.* **2015**, *7*, 5440–5470.
47. Brakenridge, G.R. Global Active Archive of Large Flood Events, Dartmouth Flood Observatory. Available online: http://floodobservatory.colorado.edu/Archives/index.html (accessed on 25 August 2015).
48. Guha-Sapir, D.; Below, R.; Hoyois, P. EM-DAT: International Disaster Database. Available online: www.emdat.be (accessed on 25 August 2015).
49. De Groeve, T.; Schmidt, R.; Raeva, L.; Dittrich, D.; Musilek, J.; Reland, M.; Vainio, T.; Nussbaum, R.; Thieken, A.; Kreibich, H.; *et al*. Guidance for Recording and Sharing Disaster Damage and Loss Data: Towards the Development of Operational Indicators to Translate the Sendai Framework into Action. Available online: http://publications.jrc.ec.europa.eu/repository/handle/JRC95505 (accessed on 25 August 2015).
50. World Meteorological Organization (WMO). First Technical Workshop on Standards for Hazard Monitoring, Data, Metadata and Analysis to Support Risk Assessment; WMO: Geneva, Switzerland, 2013.
51. NASA Tropical Rainfall Measuring Mission (TRMM). Available online: http://trmm.gsfc.nasa.gov (accessed on 25 August 2015).
52. NASA Advanced Microwave Scanning Radiometer for Earth Observation System (AMSR-E). Available online: http://aqua.nasa.gov/about/instrument_amsr.php (accessed on 25 August 2015).
53. JAXA Advanced Microwave Scanning Radiometer 2 (AMSR2). Available online: http://suzaku.eorc.jaxa.jp/GCOM_W/w_amsr2/whats_amsr2.html (accessed on 25 August 2015).
54. NASA Global Precipitation Measurement (GPM). Available online: http://pmm.nasa.gov/GPM (accessed on 25 August 2015).
55. Buizza, R.; Bidlot, J.R.; Wedi, N.; Fuentes, M.; Hamrud, M.; Holt, G.; Vitart, F. The new ECMWF VAREPS (Variable Resolution Ensemble Prediction System). *Q. J. R. Meteorol. Soc.* **2007**, *133*, 681–695.
56. Balsamo, G.; Beljaars, A.; Scipal, K.; Viterbo, P.; van den Hurk, B.; Hirschi, M.; Betts, A.K. A revised hydrology for the ECMWF model: Verification from field site to terrestrial water storage and impact in the integrated forecast system. *J. Hydrometeorol.* **2009**, *10*, 623–643.

57. Dutra, E.; Balsamo, G.; Viterbo, P.; Miranda, P.M.A.; Beljaars, A.; Schär, C.; Elder, K. An improved snow scheme for the ECMWF land surface model: Description and offline validation. *J. Hydrometeorol.* **2010**, *11*, 899–916.
58. Burek, P.; van der Knijff, J.; de Roo, A. *LISFLOOD—Distributed Water Balance and Flood Simulation Model Revised User Manual*; Technical Report for JRC: Ispra, Italy, 2013.
59. Van Der Knijff, J.M.; Younis, J.; De Roo, A.P.J. LISFLOOD: A GIS-based distributed model for river basin scale water balance and flood simulation. *Int. J. Geogr. Inf. Sci.* **2010**, *24*, 189–212.
60. Chow, V.T.; Maidment, D.R.; Mays, L.W. *Applied Hydrology*; Tata McGraw-Hill Education: New York, NY, USA, 1988.
61. Hirpa, F.A.; Salamon, P.; Alfieri, L.; Thielen, J.; Zsoter, E.; Pappenberger, F. The effect of reference climatology on global flood forecasting. *J. Hydrometeorol.* **2015**, submitted.
62. Dottori, F.; Salamon, P.; Bianchi, A.; Alfieri, L.; Feyen, L. Development and evaluation of a framework for global flood hazard mapping. *Adv. Water Resour.* **2015**, under review.
63. Dee, D.P.; Uppala, S.M.; Simmons, A.J.; Berrisford, P.; Poli, P.; Kobayashi, S.; Andrae, U.; Balmaseda, M.A.; Balsamo, G.; Bauer, P.; *et al*. The ERA-Interim reanalysis: Configuration and performance of the data assimilation system. *Q. J. R. Meteorol. Soc.* **2011**, *137*, 553–597.
64. Dottori, F.; Todini, E. Developments of a flood inundation model based on the cellular automata approach: Testing different methods to improve model performance. *Phys. Chem. Earth* **2011**, *36*, 266–280.
65. PDNA Nigeria Post Disaster Need Assessment 2012 floods. A report by The Federal Government of Nigeria. Available online: https://www.gfdrr.org/sites/gfdrr/files/NIGERIA_PDNA_PRINT_05_29_2013_WEB.pdf (accessed on 25 August 2015).
66. Hirpa, F.A.; Hopson, T.M.; De Groeve, T.; Brakenridge, G.R.; Gebremichael, M.; Restrepo, P.J. Upstream satellite remote sensing for river discharge forecasting: Application to major rivers in South Asia. *Remote Sens. Environ.* **2013**, *131*, 140–151.
67. Brakenridge, G.; De Groeve, T.; Cohen, S.; Nghiem, S.V. River Watch, Version 2: Satellite River Discharge and Runoff Measurements: Technical Summary. Available online: http://floodobservatory.colorado.edu/SatelliteGaugingSites/technical.html (accessed on 25 August 2015).
68. Alfieri, L.; Thielen, J. A European precipitation index for extreme rain-storm and flash flood early warning. *Meteorol. Appl.* **2015**, *22*, 3–13.
69. Raynaud, D.; Thielen, J.; Salamon, P.; Burek, P.; Anquetin, S.; Alfieri, L. A dynamic runoff co-efficient to improve flash flood early warning in Europe: Evaluation on the 2013 central European floods in Germany. *Meteorol. Appl.* **2015**, *22*, 410–418.
70. Modrick, T.M.; Graham, R.; Shamir, E.; Jubach, R.; Spencer, C.R.; Sperfslage, J.A.; Georgakakos, K.P. Operational Flash Flood Warning Systems with Global Applicability. Available online: http://www.hrcwater.org/about/aboutpdfs/iEMS2014_Modrick_FlashFloodWarningSystems.pdf (accessed on 25 August 2015).
71. Ward, P.J.; Jongman, B.; Salamon, P.; Simpson, A.; Bates, P.; de Groeve, T.; Muis, S.; de Perez, E.C.; Rudari, R.; Trigg, M.A.; Winsemius, H.C. Usefulness and limitations of global flood risk models. *Nat. Clim. Change* **2015**, *5*, 712–715.
72. De Groeve, T.; Poljansek, K.; Vernaccini, L. *Index for Risk Management-INFORM. Concept and Methodology. Version 2015*; European Commission: Seat, Luxembourg, 2014.

73. Bates, P.D.; Neal, J.C.; Alsdorf, D.; Schumann, G.J.P. Observing global surface water flood dynamics. *Surv. Geophys.* **2014**, *35*, 839–852.
74. Pavelsky, T.M.; Durand, M.T.; Andreadis, K.M.; Edward Beighley, R.; Paiva, R.C.D.; Allen, G.H.; Miller, Z.F. Assessing the potential global extent of SWOT river discharge observations. *J. Hydrol.* **2014**, *519*, 1516–1525.
75. Schumann, G.J.; Bates, P.D.; Di Baldassarre, G.; Mason, D.C. The use of radar imagery in riverine flood inundation studies. In *Fluvial Remote Sensing for Science and Management*; John Wiley & Sons: Chichester, UK, 2012; pp. 115–140.
76. Westerhoff, R.S.; Kleuskens, M.P.H.; Winsemius, H.C.; Huizinga, H.J.; Brakenridge, G.R.; Bishop, C. Automated global water mapping based on wide-swath orbital synthetic-aperture radar. *Hydrol. Earth Syst. Sci.* **2013**, *17*, 651–663.
77. UNITAR/UNOSAT Overview of flood waters in Mangla area, and Northern Punjab (Pakistan). Analysis with SENTINEL-1 and Landsat-8/. Available online: http://unosat-maps.web.cern.ch/unosat-maps/PK/FL20150723PAK/UNOSAT_A3_Multan_200k_portrait_20150727.pdf (accessed on 25 August 2015).
78. Posner, A.J.; Georgakakos, K.P.; Shamir, E. MODIS inundation estimate assimilation into soil moisture accounting hydrologic model: A case study in Southeast Asia. *Remote Sens.* **2014**, *6*, 10835–10859.